

Shallow Water Effect on Turning Motion of a Pusher-Barge System

Koh Kho King¹, Hironori Yasukawa² and Noritaka Hirata³

Graduate School of Engineering, Hiroshima University, 1-4-1 Kagamiyama, Higashi Hiroshima, Hiroshima, Japan 739-8527.

¹Ph.D course student, E-mail: khoking@gmail.com

²Professor, E-mail: yasukawa@naoe.hiroshima-u.ac.jp

³Assistant Professor, E-mail: nhirata@naoe.hiroshima-u.ac.jp

ABSTRACT

Nine different pusher-barge systems and eight unconventionally arranged pusher-barge systems have been studied by the authors [1][2]. This paper is a continuation to the previous studies by taking pusher-barge system (11BP) into shallow water condition. Shallow water rotating arm test (RAT) was conducted at Kyushu University with water height to ship's draught ratio (h/d) 1.2 (shallow water), 1.5 (medium shallow) and 19.3 (deep water) conditions. Hydrodynamic derivatives were obtained from the model test data by using least squares fitting method and new hydrodynamic derivative equations suitable for the three water draught ratio conditions were introduced. Linear derivatives were compared with studies from different researchers [3][4][5]. Added mass in shallow water was calculated using singularity distribution method under the assumption of rigid free surface. Propeller and rudder hull interaction parameters were pre-assumed based on the study of other researchers in shallow water condition. Pusher-barge 11BP is found to have negative course stability index in shallow water condition, which means the pusher is unstable. Maneuvering simulations were performed at 20 degrees and 35 degrees turning. Pusher-barge 11BP is found to have the largest turning circle in deep water and smallest turning circle in shallow water condition. Course keeping ability decreases from deep to medium shallow to shallow water conditions.

KEY WORDS: Pusher-barge; shallow water effect; turning motion.

1 INTRODUCTION

Pusher-barge systems are commonly being used in inland waterways, where water depth often is of limitation. In ship maneuvering, water depth plays an important role, where different water depth will result different turning characteristics of a vessel. Nine different pusher-barge systems [1] and eight unconventionally arranged pusher-barge systems [2] were studied by the authors.

As a continuation to the pusher-barge study, shallow water effect in maneuvering was investigated in this paper. Pusher-barge system, 11BP, was taken as the subject of the study and shallow water tests were conducted at Kyushu University. Hydrodynamic derivatives were obtained by least squares fitting to the model test data. Maneuvering simulations were performed based on the captured hydrodynamic derivatives and also some pre-assumed propeller and rudder hull interaction parameters with referred to the study of other researchers. These were discussed in more details in the later sections.

2 SHIP MODEL

Principal particulars of the pusher and barge in model scale and full-scale used in the research are shown in Table 1. Fig. 1 shows the body plan of the pusher and barge used. Pusher used in the model test is without propeller and rudder installed. However, in the simulation pusher used is assumed to be twin screws and twin rudders. Controllable pitch propeller (CPP) is assumed to be installed with diameter (D_P) 1.8m and revolution 300rpm. Main engine power is 1000kW. Rudder span is 2.0m, cord 2.0m and area (A_R) 4.0m². Pusher design and specifications are with referred to reference [6].

Rake-barge with ship like design at the bow was used in the study. Bow part of the rake-barge is curved and sharp with water piercing design. Table 1 shows the principal dimensions of the rake-barge. Body plan of the rake-barge is shown in Fig. 1. In

this paper, one pusher and one barge were used as the subject of the study. One rake-barge and a pusher were arranged in-line, named "11BP". Table 2 shows the principal dimensions of pusher-barge 11BP, where LOA is the length overall of the system, B is the maximum breadth, d is the water draught, and C_b is the block coefficient with regards to the LOA, B and d of the system. Fig. 2 shows the photo of the actual model of 11BP pusher-barge system used in the model experiment. Scale ratio of the model is 1/50. Propellers and rudders were not installed during the experiment.

Table 2: Principal dimensions of the pusher-barge system in full-scale

symbol	11BP
LOA (m)	100.96
B (m)	10.67
d (m)	2.74
∇ (m ³)	2140.9
LCB from AP (m)	58.47
C_b	0.725

3 HYDRODYNAMIC DERIVATIVES CHARACTERISTICS

3.1 Captive Model Test

In order to obtain shallow water hydrodynamic derivatives, rotating arm test (RAT) was performed at Kyushu University square tank. In the experiments, three different water depth to ship's draught ratios were performed, where $h/d = 19.3$ (deep water), 1.5 (medium shallow) and 1.2 (shallow water). Water was drained from the tank in order to get the desired water height to model's draught ratio. Model's trim, draught and roll motions

Table 1: Principal dimensions of the pusher and barge

	pusher		rake-barge	
	Full-scale	Model	Full-scale	Model
Length Overall, LOA (m)	40.00	0.80	60.96	1.22
Length btw. Perpendiculars, LBP (m)	39.50	0.79	60.96	1.22
Breadth, B (m)	9.00	0.18	10.67	0.21
Draft, d (m)	2.20	0.044	2.74	0.055
Volume, ∇ (m ³)	494.7	0.00396	1646.2	0.01317
LCB from AP (m)	21.98	0.4395	29.44	0.5888
Block Coefficient, C_b	0.633	0.633	0.924	0.924

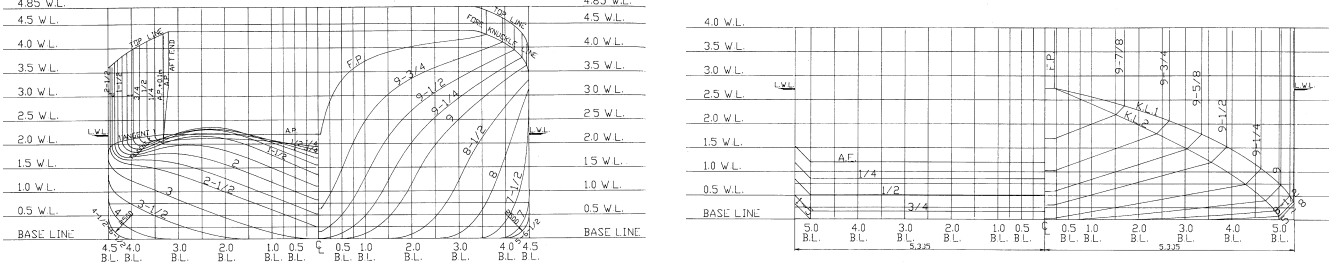


Fig. 1: Body plans of the pusher and the rake-barge

were fixed. Model forward speed, $U = 0.364\text{m/s}$, is equivalent to full-scale ship's speed of 5 knots. During the experiments, force and moment transducer was used and placed at the mid-ship of the pusher-barge model. Longitudinal force (X_H^*), lateral force (Y_H^*) and yawing moment (N_H) were recorded and non-dimensionalized using the following equations:

$$X_H', Y_H' = \frac{X_H^*, Y_H^*}{(1/2)\rho LOA dU^2} \quad (1)$$

$$N_H' = \frac{N_H}{(1/2)\rho LOA^2 dU^2} \quad (2)$$

In the equation, LOA is the length overall of the pusher-barge system, ρ is water density, d is model's draught, and U is the forward speed. "*" denotes results measured from experiments with virtual mass influence included. No correction was needed for N_H due to virtual mass, hence N_H was used directly in the equation. Since, forces and moment measured from the experiments are having added mass influences included, they must be calculated separately and be excluded when processing the experiment data.

3.2 Added Mass Coefficients

Added mass coefficients in shallow water were calculated using singularity distribution method with the assumption of rigid free-surface. Fig. 3 shows the shallow water effect on added mass. From Fig. 3, it is found that added mass reduced increased significantly when h/d approaches 1. Added mass were non-dimensionalized (m'_{11} , m'_{22} , m'_{26} , m'_{66}) using the following equations:

$$m'_{11}, m'_{22} = \frac{m_{11}, m_{22}}{(1/2)\rho LOA^2 d} \quad (3)$$

$$m'_{26} = \frac{m_{26}}{(1/2)\rho LOA^3 d} \quad (4)$$

$$m'_{66} = \frac{m_{66}}{(1/2)\rho LOA^4 d} \quad (5)$$

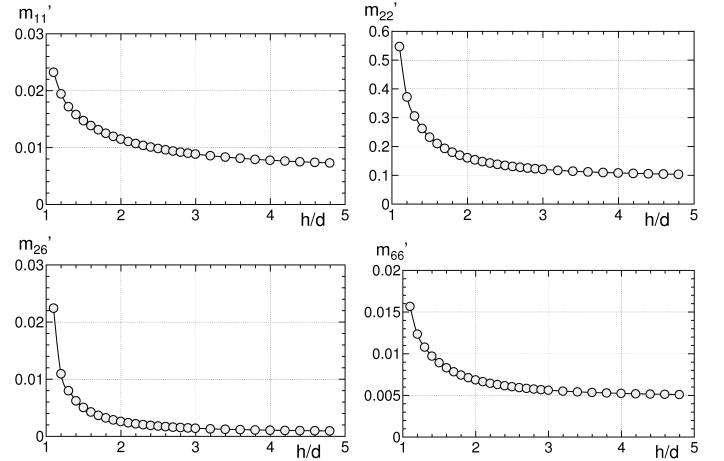


Fig. 3: Shallow water effect on added mass coefficients for 11BP

3.3 Model Experiment Results of Hydrodynamic Derivatives

Experimental results of longitudinal force, lateral force and yawing moment in non-dimensional form (X_H' , Y_H' , N_H') were plotted in Fig. 4. Circle, triangle, square and diamond shapes are data obtained from experiments. Intermediate lines in the figure are fitting using hydrodynamic derivatives obtained from lead square method. In general, hydrodynamic derivatives for shallow water, medium shallow water and deep water are having the same plot trend. However, for $h/d = 1.2$, at 20 degrees oblique drift angle, Y_H' has a drop or reduction in force. From the experiment data,

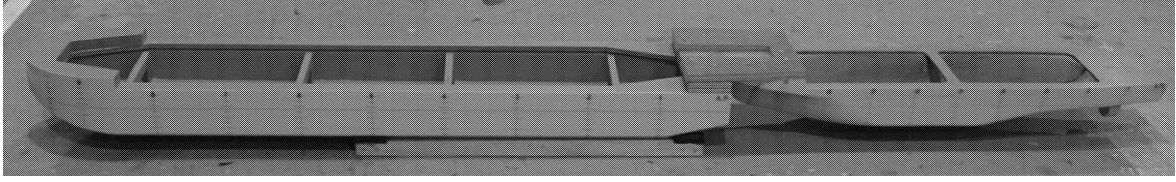


Fig. 2: Model of pusher-barge 11BP

second order equation for X'_H with respect to β_m and r' and third order equation for Y'_H and N'_H were derived, as shown in Eq. (6).

$$\left. \begin{aligned} X'_H &= X'_0 \cos^2 \beta_m + X'_{\beta\beta} \beta_m^2 + X'_{\beta r} \beta_m r' \\ &\quad + X'_{rr} r'^2 \\ Y'_H &= Y'_{\beta} \beta_m + Y'_r r' + Y'_{\beta\beta} \beta_m^3 + Y'_{\beta r} \beta_m^2 r' \\ &\quad + Y'_{\beta rr} \beta_m r'^2 + Y'_{rrr} r'^3 \\ N'_H &= N'_{\beta} \beta_m + N'_r r' + N'_{\beta\beta} \beta_m^3 + N'_{\beta r} \beta_m^2 r' \\ &\quad + N'_{\beta rr} \beta_m r'^2 + N'_{rrr} r'^3 \end{aligned} \right\} \quad (6)$$

In the equation, β_m is the oblique drift angle at midship, r' is the non-dimensional turning rate ($r' \equiv rL/U$), X'_0 is the forward resistance, $X'_{\beta\beta}$, Y'_{β} , etc. are the hydrodynamic derivatives. In the previous study [1], $Y'_{\beta rr}$ and Y'_{rrr} were neglected due to the limited turning rate in the experiment, making accuracy of higher order of r' difficult to obtain. However, in this paper, shallow water tests were conducted till $r' = 0.7$, fitting in Fig. 4 shows satisfactory results for practical use. From Fig. 4, hydrodynamic derivatives for maneuvering were decided, where for $h/d = 19.3$ and 1.5, the obtained hydrodynamic derivatives are good for all drift angle as tested in the study, but for $h/d = 1.2$ the obtained hydrodynamic derivatives are limited to drift angle -5 degrees till 15 degrees. Hydrodynamic derivatives obtained from the experiments and used in this paper are shown in Table 3. In Table 3, added mass coefficients are shown as well.

Table 3: Resistance coefficient, hydrodynamic derivatives and added mass coefficients

symbol	$h/d = 19.3$	$h/d = 1.5$	$h/d = 1.2$
$X'_{\beta\beta}$	-0.053	-0.1749	-0.3637
X'_{rr}	0.0272	0.0792	0.1055
$X'_{\beta r} - m'_{22}$	-0.1069	-0.3213	-0.6202
Y'_{β}	0.221	0.6354	1.2375
$Y'_r - m'_{11}$	-0.0151	-0.0375	-0.1325
$Y'_{\beta\beta\beta}$	0.4857	2.5353	4.2245
$Y'_{\beta\beta r}$	-0.2268	0.7413	3.6005
$Y'_{\beta rr}$	0.1562	0.286	0.7129
Y'_{rrr}	0.0118	-0.0836	-0.2003
N'_{β}	0.0706	0.1988	0.4435
N'_r	-0.0593	-0.0654	-0.0861
$N'_{\beta\beta\beta}$	0.0848	0.5665	1.1277
$N'_{\beta\beta r}$	-0.1407	-0.6547	-0.2249
$N'_{\beta rr}$	0.0358	-0.0528	-0.0561
N'_{rrr}	0.0028	0.0097	-0.0522
m'_{11}	0.0195	0.0148	0.006
m'_{22}	0.3722	0.2325	0.0929
$m'_{2\beta}$	0.0108	0.005	0.0006
m'_{66}	0.0124	0.0089	0.0049

3.4 Linear Hydrodynamic Derivatives and Course Stability

Linear derivatives obtained from the experiments, Y'_{β} , Y'_r , N'_{β} , N'_r , were compared with papers published by other researchers in shallow water studies. Pusher-barge system 11BP at different water depth ratio were compared with the linear derivatives of PCC [4], LNGC [3], Wide-beam Twin [5], and Conventional Twin [5]. Fig. 5 shows the shallow water effect on linear hydrodynamic derivatives. From the figure, it is found that for $Y_{\beta}/Y_{\beta-deep}$, pusher-barge 11BP is having similar changes of the derivatives from deep to shallow water as LNGC. From $N_{\beta}/N_{\beta-deep}$ plot, pusher-barge 11BP is having similar trend between PCC and wide beam twin vessels. In Y_r/Y_{r-deep} plot, pusher-barge 11BP show very high value of Y_r/Y_{r-deep} in medium shallow and shallow water conditions and is much higher than the other type of vessels. Plot of N_r/N_{r-deep} shows 11BP with significantly lower value of N_r/N_{r-deep} in medium shallow and shallow water conditions as compared to other vessels.

Course stability index, C , is defined in Eq. (7). Rudder effect is not taken into account in C calculation. Negative value of course stability index in shallow water condition shows that pusher-barge 11BP is unstable in course keeping in shallow water.

$$C = \frac{N'_r}{Y'_r - m' - m'_{11}} - \frac{N'_{\beta}}{Y'_{\beta}} \quad (7)$$

In analysing the effect of water depth on course stability, changes of $N'_r/(Y'_r - m' - m'_{11})$, N'_{β}/Y'_{β} and C versus d/h were plotted as shown in Fig. 6. From the figure, for 11BP, it is found that at shallow water, value of $N'_r/(Y'_r - m' - m'_{11})$ drops while N'_{β}/Y'_{β} increases. This resulted in the negative value of C , lead to unstable course keeping ability of the vessel. Wide beam twin and conventional twin have similar course keeping behavior, while PCC has different behavior than the rest of the vessels.

Table 4: Resistance coefficient, hydrodynamic derivatives, added mass, and course stability index

symbol	$h/d = 19.3$	$h/d = 1.5$	$h/d = 1.2$
$N'_r/(Y'_r - m' - m'_{11})$	0.3521	0.3428	0.3013
N'_{β}/Y'_{β}	0.3195	0.3129	0.3584
C	0.0327	0.0299	-0.0571

4 TURNING SIMULATION

4.1 Simulation Outline

In order to understand more clearly the maneuvering behavior of pusher-barge system 11BP in different water depths, turning simulation of 20 degrees and 35 degrees rudder angle was carried

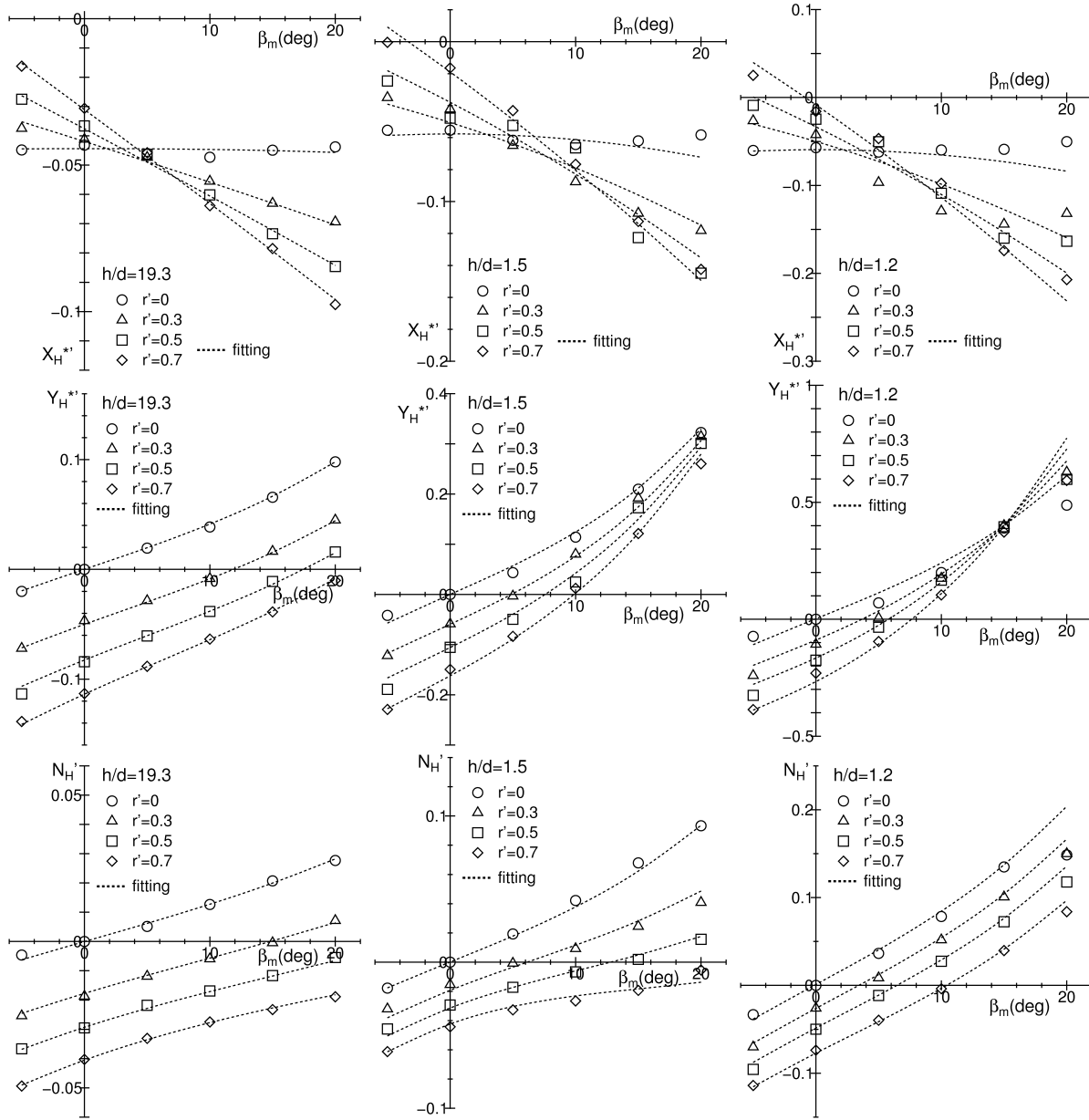


Fig. 4: Hydrodynamic force characteristics for 11BP in $h/d=19.3, 1.5, 1.2$

out. Wind, wave and current effects were not taken into consideration in the simulations. Propeller revolution is set at 300RPM and pusher-barge forward speed at 5 knots. Twin screws, twin rudders and controllable pitch propellers (CPP) were used in the simulations. Propellers and rudders were arranged symmetrically on port and starboard. Pusher-barge 11BP has identical port and starboard turn due to the symmetrical arrangement of hull, propellers and rudders, hence only starboard turn is performed in the simulations. Hydrodynamic derivatives from the previous section are used in the simulations. Detail of the simulation calculations is shown in the appendix.

Propeller, rudder and hull interaction parameters used in the simulations are shown in Table 5 (symbols used in the table are explained in the appendix). For $h/d=19.3$ deep water case, the parameters used are the same as in papers [1] and [2]. For medium shallow water ($h/d=1.5$) and shallow water ($h/d=1.2$) conditions,

twin screws wide beam ship as in [5] was referred. γ_R coefficient is with referred to Yoshimura paper in [4].

Model resistance obtained from the experiments is having a tendency of decreasing in resistance from deep to medium shallow to shallow water. This contradicted with the findings in studies done by other researchers [7][8][9]. Hence model resistance of deep water from paper [2] of the same pusher-barge 11BP was used. Medium shallow water and shallow water resistance was corrected based on the deep water resistance using Lackenby correction as suggested by ITTC [10]. As pusher-barge 11BP was moving at slow speed, it falls under sub-critical region for wave resistance correction, hence no correction for wave resistance is needed [9].

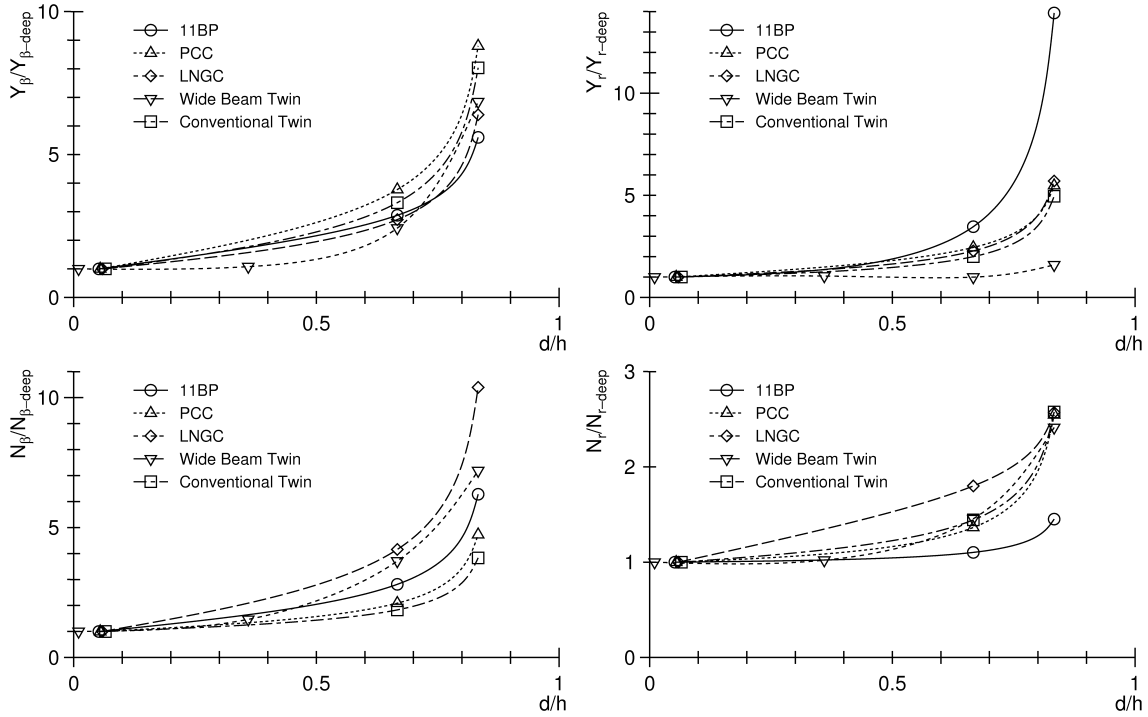


Fig. 5: Shallow water effect on linear derivatives of different ship types

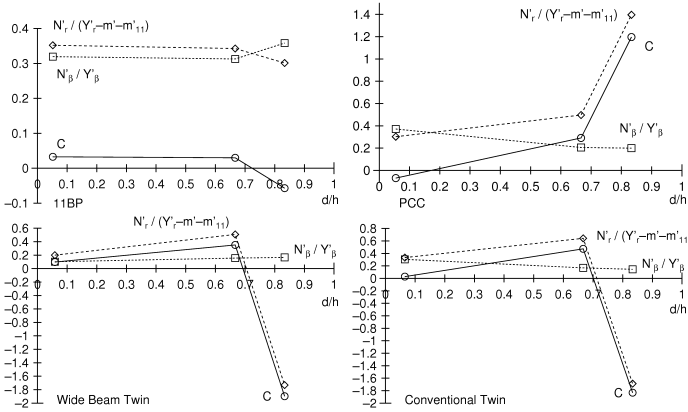


Fig. 6: Course stability index

4.2 Calculation Results

Turning trajectories of pusher-barge 11BP with 20 degrees and 35 degrees rudder angle starboard turning at different water depths are presented in Fig. 7 and 8. Tactical diameter and advance of

Table 5: Extra parameters used in the simulation

symbol	$h/d = 19.3$	$h/d = 1.5$	$h/d = 1.2$
t	0.164	0.249	0.326
a_H	0.194	0.089	0.418
x'_H	-0.427	-0.249	-0.189
w_{P0}	0.340	0.493	0.576
γ_R	0.230	0.357	0.293
ℓ_R	-1.033	-0.538	-1.113
ε	0.987	1.189	1.823

the various water depth conditions are presented in Figs. 9 and 10.

Fig. 7 shows turning trajectories of pusher-barge 11BP at 20 degrees rudder angle in deep, medium shallow and shallow water conditions. From Fig. 7, pusher-barge 11BP is having the largest turning trajectory in deep water, followed by medium shallow and shallow water conditions. Yasukawa [11] and Yoshimura [5] found that for wide beam vessel, turning circle decreases from deep to shallow water; whereby for conventional vessel, turning circle increases from deep to shallow water. Pusher-barge 11BP is having similar to wide beam vessel in turning performance. Fig. 8 shows similar turning performance at rudder angle 35 degrees as compared to 20 degrees for pusher barge 11BP in deep, medium shallow and shallow water conditions.

To further analyze the turning simulation results, free running model test of similar arrangement of pusher-barge 11BP with rudder angle 35 degrees conducted in Indonesian Hydrodynamic Laboratory (IHL) [12] was compared. Results from IHL shows that advance increases slightly from $h/d=1.1$ to $h/d=2.0$. For tactical diameter, the value is almost constant throughout the h/d ratio from 1.1 to 2.0. The results match the simulation results of $\delta = 35$ degrees in Fig. 9.

In analyzing the turning behavior of pusher-barge 11BP from deep water to medium shallow water to shallow water, rudder force in the three water depth conditions was studied. Fig. 11 shows the rudder force plot in time series for pusher-barge 11BP in 20 degrees and 35 degrees rudder angle for deep, medium shallow and shallow water conditions. From the figure, it can be seen that shallow water and medium shallow water cases have significantly higher rudder force by nearly 100% increment. This resulted in better turning performance of the pusher barge system in medium shallow and shallow water conditions than in deep water.

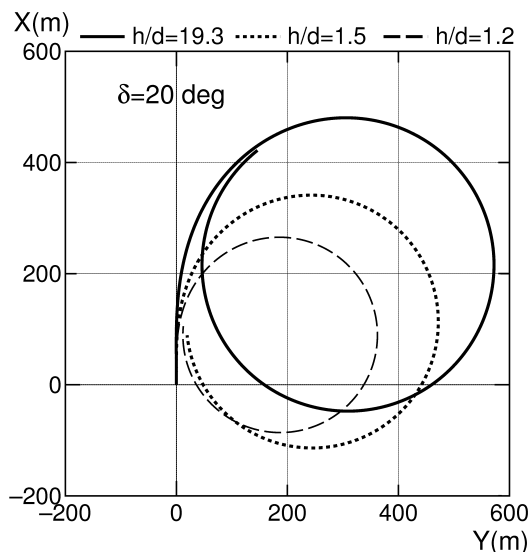


Fig. 7: Turning trajectories ($\delta = 20$ deg)

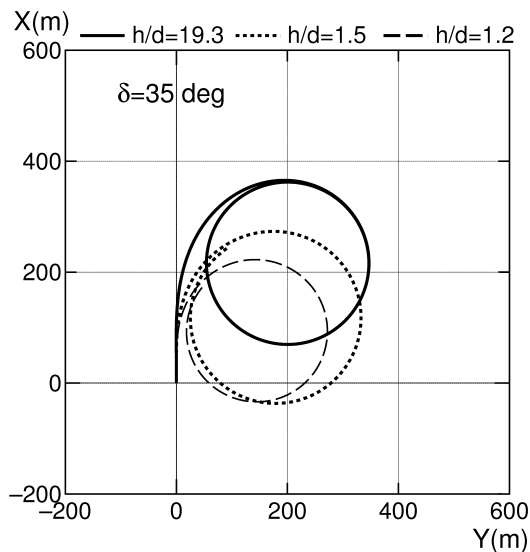


Fig. 8: Turning trajectories ($\delta = 35$ deg)

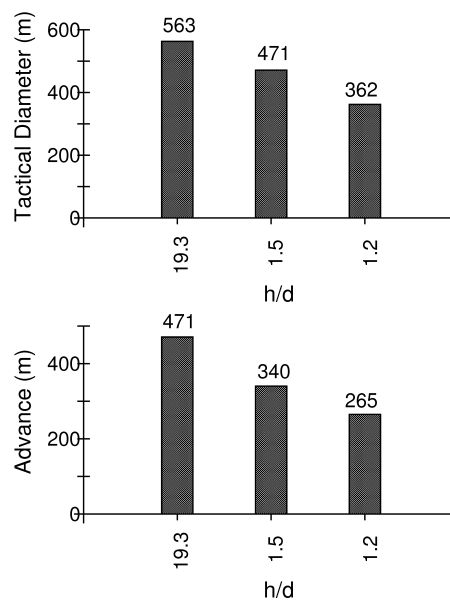


Fig. 9: Tactical diameter and advance distance ($\delta = 20$ deg)

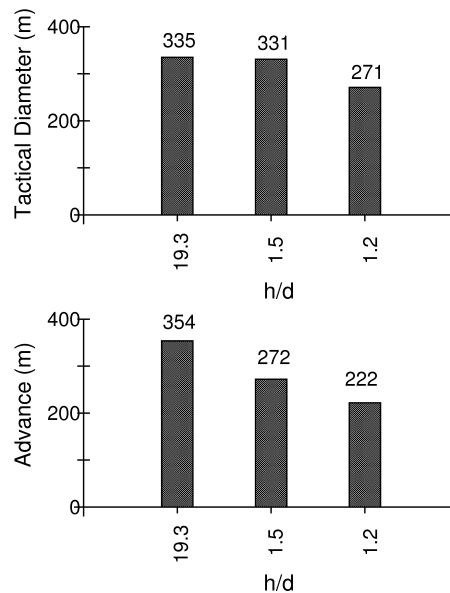


Fig. 10: Tactical diameter and advance distance ($\delta = 35$ deg)

5 CONCLUDING REMARKS

Pusher-barge system with one pusher and one barge arranged in-line (11BP) has been studied in study. Rotating arm test was carried out in three water depth to ship's draught conditions ($h/d = 19.3$ (deep water); 1.5 (medium shallow); 1.2 (shallow water)). In shallow water condition, pusher-barge 11BP is found to have negative value of course stability index (C), which means that the system is not stable in course keeping. Pusher-barge 11BP is having the largest value of C in deep water, which is the easiest to maneuver condition among the three water depth to ship's draught ratios.

In turning simulations, for rudder angle 20 degrees, pusher-barge 11BP turning performance is similar to a wide beam vessel, where turning trajectory decreases from deep to medium shallow to shallow water condition. For rudder angle 35 degrees, pusher-barge 11BP is having the similar performance as 20 de-

grees rudder angle, where largest turning circle occurs in deep water, followed by medium shallow and then shallow water. The authors also found big increment in rudder force from deep to medium shallow and shallow water conditions.

For future work, the authors suggest conducting free running model test on pusher-barge systems in comparison with the computer simulations. Different combinations and arrangements of pusher-barge system should also be tested and simulated for a better understanding of pusher-barge maneuvering characteristics in shallow water.

ACKNOWLEDGEMENT The authors want to thank emeritus Professor K. Kijima of Kyushu University for providing the facilities and assistance in conducting the rotating arm

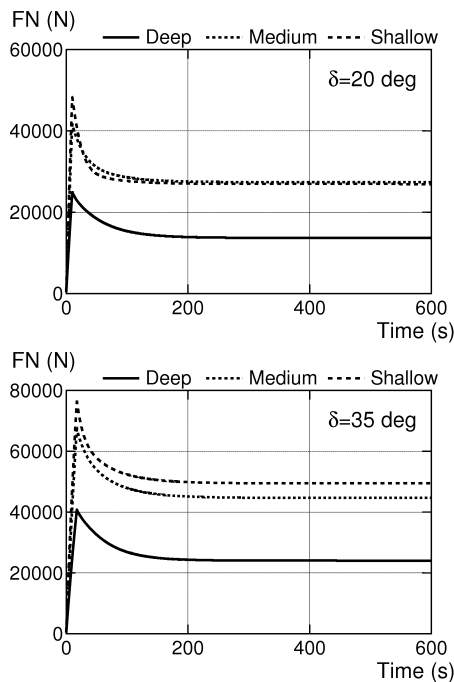


Fig. 11: Rudder force changes in time series for deep, medium shallow and shallow water conditions

test in various water depths conditions.

References

[1] Yasukawa H, Hirata N, Koh KK, Punayangkool K, Kose K (2007). "Hydrodynamic Force Characteristics on Maneuvering of Pusher-Barge Systems (in Japanese)," *J Jpn Soc Nav Archit Ocean Eng*, Vol 5, pp 133-142.

[2] Koh KK, Yasukawa H, Hirata N, Kose K (2008). "Hydrodynamic Derivatives Investigation on Unconventionally Arranged Pusher-Barge Systems," *J Mar Science Tech* (to be published).

[3] Fujino M, Ishiguro T (1984). "A Study of the Mathematical Model Describing Maneuvering Motions in Shallow Water. Shallow water effects on rudder-effectiveness parameters (in Japanese)," *J Soc Nav Archit Jpn*, Vol 156, pp 18-192..

[4] Yoshimura Y (1986). "Mathematical Model for the Manoeuvring Ship Motion in Shallow Water (in Japanese)," *J Kansai Soc Nav Archit Jpn*, Vol 200, pp 41-51.

[5] Yoshimura Y, Sakurai H (1989). "Mathematical Model for the Manoeuvring Ship Motion in Shallow Water (3rd Report) (in Japanese)," *J Kansai Soc Nav Archit Jpn*, Vol 211, pp 115-126.

[6] Pfennigstorf J (1970). "Handbuch der Werften X Band," *Bearb von K Wendel, Schifffahrts-Verlag HANSA, C Schroedter & Co, Hamburg* 11.

[7] Millward A (1982). "The Effect of Shallow Water on the Resistance of Ship at High Sub-Critical and Super-Critical Speeds," *Trans RINA*, Vol 124, pp 175-181.

[8] Millward A (1991). "A Comparison of the Effects of Restricted Water Depth on a Model and Full Size Planning Hull," *Trans RINA*, Vol 133, pp 237-250.

[9] Hofman M (2000). "Shallow Water Resistance Charts for Preliminary Vessel Design," *Int Shipbuilding Prog*, Vol 31, No 449, pp 61-76.

[10] Lackenby H (1963). "The Effect of Shallow Water on Ship Speed," *Shipbuilder* Vol 70, No 672.

[11] Yasukawa H, Kobayashi E (1995). "Shallow Water Model Experiments on Ship Turning Performance," Mini Symposium on Ship Manoeuvrability 26 May 1995, *West-Japan Soc Nav Archit*, pp 71-83.

[12] Yasukawa H (eds) (2006). "Study on River Transportation by Pusher and Multi-Barge System," *The Report of 11th Seminar of JSPS-DGHE Core University Program on Marine Transportation Engineering*, Hiroshima University, No 06-1, pp 444.

[13] Hirano M (1980). "On the Calculation Method of Ship Maneuvering Motion at the Initial Design Phase (in Japanese)," *J Soc Nav Archit Jpn*, Vol 147, pp 144-153.

[14] Fujii H, Tuda T (1961). "Experimental Research on Rudder Performance (2) (in Japanese)," *J Soc Nav Archit Jpn*, Vol 110, pp 31-42.

[15] Yoshimura Y, Nomoto K (1978). "Modeling of Maneuvering Behaviour of Ships with a Propeller Idling, Boosting and Reversing (in Japanese)," *J Soc Nav Archit Jpn*, Vol 144, pp 57-69.

A Maneuvering Simulation Calculations

Fig. 12 shows the coordinate systems used in the paper. $O - X_0Y_0Z_0$ are the space coordinate system, with X_0Y_0 as to the water surface and Z_0 vertically downwards axis from the water surface. ψ is the angle from X_0 axis to the center of gravity of the ship. $G - xyz$ is the ship's coordinate system, where G is the center of gravity of the ship, x is the forward direction of the ship and y is the lateral direction of the ship. xy forms the water surface where the ship is located and z is the vertical downwards direction from the center of gravity of the ship.

Maneuvering motions of the pusher-barge system (surge, sway, yaw) are defined in the motion equations shown in Eq. (8). In the equation, $\dot{}$ is time based of the respective parameters. The unknown values are: u the forward speed, v the lateral speed and r the turning rate. m is the mass of the ship and I_{zz} is the moment inertia of the ship. m_{11} , m_{22} , m_{26} , m_{66} are the added mass and added moment of inertia of the pusher-barge system that occur when a ship accelerate or decelerate or in turning motion. On the right hand side of the equation, X is the total forward force, Y is the total lateral force and N is the total yaw moment at the center of gravity of the pusher-barge system.

$$\left. \begin{aligned} (m + m_{11})\dot{u} - (m + m_{22})vr &= X \\ (m + m_{11})ur + (m + m_{22})\dot{v} + m_{26}\dot{r} &= Y \\ (I_{zz} + m_{66})\dot{r} + m_{26}\dot{v} &= N \end{aligned} \right\} \quad (8)$$

X , Y , and N are the forces and moment introduced from hull (H), propeller (P) and rudder (R), which are expressed in Eq.

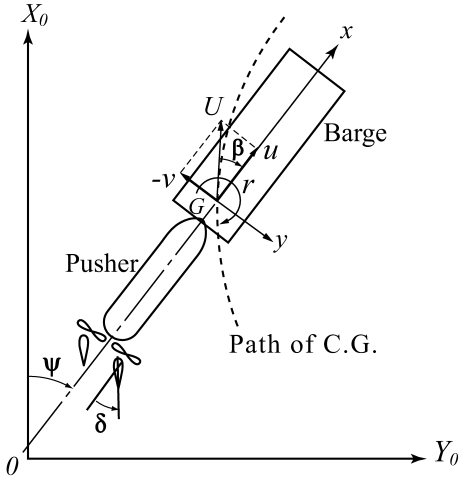


Fig. 12: Coordinate systems

(9).

$$\left. \begin{aligned} X &= X_H + X_P + X_R \\ Y &= Y_H + Y_R \\ N &= N_H + N_R - (Y_H + Y_R)x_G \end{aligned} \right\} \quad (9)$$

In model tank test, measurement was done at the midship of the pusher-barge system, while longitudinal force X is unaffected, but lateral force Y and moment N need to be corrected from midship to the center of gravity of the pusher-barge system. The relationship of lateral velocity at midship v_m to the lateral velocity at center gravity of the pusher-barge system v is shown in Eq. (10). The midship drift angle β_m is defined in Eq. (11).

$$v_m = v - x_G r \quad (10)$$

$$\beta_m = \tan^{-1} \left(\frac{-v_m}{u} \right) \quad (11)$$

Hydrodynamic force that acts on a hull when a ship makes a diagonal turn is mainly caused by the dynamic pressure of the fluid. If the flow along a hull is to be related to the ship's length, and the displacement of the hull is to be related to the draught of the ship, then the flow and pressure can be related to $LOA \times d$. Hydrodynamic force (X_H, Y_H, N_H) on ship's hull based on the above consideration is shown in Eq. (12). In the equation, U is the ship's speed ($U = \sqrt{u^2 + v^2}$). X'_H, Y'_H, N'_H are defined in Eq. (6).

$$\left. \begin{aligned} X_H &= (1/2)\rho LOA dU^2 X'_H(\beta_m, r') \\ Y_H &= (1/2)\rho LOA dU^2 Y'_H(\beta_m, r') \\ N_H &= (1/2)\rho LOA^2 dU^2 N'_H(\beta_m, r') \end{aligned} \right\} \quad (12)$$

Propeller at aft of the pusher-barge system only contributing force in the X direction. Total force produced by the propeller as experienced by a ship is defined as:

$$X_P = (1-t) \sum T \quad (13)$$

where t is the thrust deduction factor and $\sum T$ is the total thrust produces by the propellers (twin screws in this study).

$$T = \rho n_P^2 D_P^4 K_T(J_P, p) \quad (14)$$

In Eq. (14) D_P is the propeller diameter, K_T is the thrust coefficient, J_P is the propeller advanced coefficient, and p is the

propeller pitch ratio. K_T and J_P are defined in Eq. (15) and Eq. (16).

$$K_T(J_P, p) = -0.3260pJ_P - 0.2005J_P + 0.5234p - 0.0398 \quad (15)$$

$$J_P = \frac{u(1-w_P)}{n_P D_P} \quad (16)$$

In Eq. (16), w_P is the propeller wake fraction which change accordingly with the drift angle β and also the non-dimensional ship turning rate r' . Hirano's formula [13] was used in calculating the propeller wake fraction.

$$w_P = w_{P0} \exp[C_1 \beta_P^2] \quad (17)$$

where w_{P0} is the wake factor during the forward speed of the pusher-barge system, β_P is the drift angle at the propeller position ($\equiv \beta - \ell_P r'$), and C_1 is the correction factor. Rudder forces (X_R and Y_R) and moment (N_R) are defined in Eq. (18).

$$\left. \begin{aligned} X_R &= -\sum F_N \sin \delta \\ Y_R &= -(1+a_H) \sum F_N \cos \delta \\ N_R &= -(x_R + a_H x_H) \sum F_N \cos \delta \end{aligned} \right\} \quad (18)$$

where δ is the rudder angle, a_H and x_H are the rudder and hull interaction parameters, and x_R is the x -coordinate point on which the rudder force F_N acts. F_N is defined as below:

$$F_N = \frac{1}{2} \rho A_R U_R^2 f_\alpha \sin \alpha_R \quad (19)$$

In the equation, A_R is rudder area and f_α is gradient of the lift coefficient of the rudder. f_α is estimated using Fujii's formula[14]. U_R is the flow velocity to the rudder and α_R is the effective rudder in-flow angle:

$$U_R = \sqrt{u_R^2 + v_R^2} \quad (20)$$

$$\alpha_R = \delta - \tan^{-1} \left(\frac{v_R}{u_R} \right) \quad (21)$$

In Eq. (20), u_R is the water flow speed towards the rudder and v_R is the lateral flow speed after passing the propeller. v_R is calculated using Eq. (22) which is related to the rudder location and is influenced by the geometrical inflow angle to the rudder β_R ($\equiv \beta - \ell'_R r'$), and γ_R is the flow-rectification coefficient to the rudder.

$$v_R = U \gamma_R \beta_R \quad (22)$$

u_R is defined using Yoshimura's formula[15]:

$$u_R = \frac{\varepsilon u_P}{1-s} \sqrt{1 - 2(1-\eta\kappa)s + \{1 - \eta\kappa(2-\kappa)\}s^2} \quad (23)$$

where s is the propeller slip ratio, η is the ratio of propeller diameter with rudder height, κ is the propeller flow correction factor ($\kappa = 0.6/\varepsilon$ is normally used in deep water case), and ε is the flow coefficient of the rudder with respect to its location.